

P194

Gradient Calculations for 3D Inversion of CSEM Data Using a Fast Finite-difference Time-domain Modelling Code

T. Støren* (EMGS), J.J. Zach (EMGS) & F.A. Maaø (EMGS)

SUMMARY

Gradient-based 3D inversion of controlled-source electromagnetic (CSEM) data requires the gradient to a data-misfit functional to be computed within the volume where we seek to find a resistivity model that explains the observed data. Since 3D inversion typically requires more than 100 iterations in order to converge to a good model, fast modelling is important to make 3D inversion a feasible tool in advanced interpretation of CSEM data. We have previously presented a fast finite-difference time-domain (FDTD) modeling code which reduces the computational time of a typical modelling scenario by a factor of 40. In this presentation we show how we use this FDTD modeling to efficiently compute the misfit gradient. A benefit of this approach is that the gradient can be computed for several frequencies in one forward modelling thus saving valuable computational resources when inverting data from a large number of receivers. We present results showing that the gradients obtained are well-behaved. We also present results from inversion of synthetic data based on these gradient calculations showing that, for this specific example, a good result was obtained for the inverted resistivity model after relatively few iterations.

Introduction

Marine controlled-source electromagnetic (CSEM) surveying has been used for geophysical investigations since 1979 (Spies et al., 1980). Since hydro-carbon bearing sediments tend to have higher resistivity than water-saturated sediments CSEM measurements are sensitive to the presence of sub-surface hydro-carbons. During recent years the method has been put into use for offshore petroleum exploration (Eidesmo et al., 2002).

For complex geological settings, e.g. presence of hydrates or other resistive formations or large variations in bathymetry, the classic interpretation of CSEM data, where anomalies are identified by comparing the electromagnetic responses to a reference response, can be challenging. The aim of 3D inversion of CSEM data is to obtain a three-dimensional resistivity model of the subsurface which explains the observed data. The problem is inherently ill-conditioned, but combined with knowledge about geology, and possibly combined with other types of data, e.g. through various joint-inversion approaches, inversion is expected to become an important tool for advanced interpretation of CSEM data.

Inversion is often implemented as an iterative process, where the resistivity model is modified in each iteration seeking to minimize the misfit between observed data and synthetic data computed based on the current model at that point in the inversion process (e.g. Newmann and Alumbaugh, 1997). Various methods for minimizing the misfit have been applied to CSEM data, e.g. Marquard-Levenberg optimization (Mittet et al. 2004), simulated annealing (Roth and Zach, 2007), regularized focusing inversion (Gribenko and Zhdanov, 2007). For complex geological settings with no or little prior knowledge, where full 3D models are necessary to explain observed data, local gradient-based optimization is currently the only published feasible solution (Plessix and van der Sman, 2007).

Gradient-based inversion

Omitting regularization terms often used to constrain the inversion, a typical misfit functional based upon electromagnetic field data only is

$$\varepsilon = \sum_{s,r,\omega,F} W^F \Delta F_i(\vec{x}_r|\vec{x}_s;\vec{J},\omega) \Delta F_i^*(\vec{x}_r|\vec{x}_s;\vec{J},\omega) = \sum_{r,\omega,F} \mathcal{E}^F(\vec{x}_r,\omega;\vec{J}), \quad (1)$$

where we \mathcal{E}^F denotes the kernel of the misfit functional. The sum is over source and receiver positions, frequency, and fields. $F_i = \{E_i, H_i\}$, is a component of the electric or magnetic field in direction i . Repeated indices indicate a summation over the field components. The difference field is defined as

$$\Delta F_i(\vec{x}_r|\vec{x}_s;\vec{J},\omega) \Big|_{\sigma(\vec{x})} = F_i^{obs}(\vec{x}_r|\vec{x}_s;\vec{J},\omega) - F_i^{synth}(\vec{x}_r|\vec{x}_s;\vec{J},\omega) \Big|_{\sigma(\vec{x})}, \quad (2)$$

where F_i^{obs} is the field observed at receiver position \mathbf{x}_r , in response to a source \mathbf{J} at position \mathbf{x}_s . F_i^{synth} is the corresponding synthetic field for the conductivity model $\sigma(\mathbf{x})$. The weight function W^F is needed to balance contributions from fields at different offsets to the misfit functional. It can also be interpreted as being inversely proportional to data uncertainty. A simple weight function is the inverse squared amplitude of the observed field.

When the conductivity model changes slightly at position \mathbf{x} , the synthetic field at the receiver position changes accordingly, leading to a change in the misfit functional. Within the first Born approximation, the field perturbation δF^{synth} due to a model perturbation $\delta\sigma(\mathbf{x})$ can be expressed as

$$\delta F_i^{synth}(\vec{x}_r|\vec{x}_s;\vec{J},\omega) \Big|_{\sigma(\vec{x})+\delta\sigma(\vec{x})} \approx \sum_{\vec{x}} G_{in}^{FJ}(\vec{x}_r|\vec{x};\omega) G_{nk}^{EJ}(\vec{x}|\vec{x}_s;\omega) J_k(\vec{x}_s;\omega) \delta\sigma(\vec{x}). \quad (3)$$

To the first order in the model change, the gradient of the misfit functional with respect to a change in the conductivity model can then be written

$$\frac{\delta \mathcal{E}^F(\vec{x}_r,\omega)}{\delta\sigma(\vec{x})} \approx \pm G_{ni}^{ES}(\vec{x}|\vec{x}_r;\omega) \sum_s G_{nk}^{EJ}(\vec{x}|\vec{x}_s;\omega) W^F(\vec{x}_r|\vec{x}_s;\omega) \Delta F_i^*(\vec{x}_r|\vec{x}_s;\vec{J},\omega) J_k(\vec{x}_s;\omega) + C.C., \quad (4)$$

where the G 's denote Green's functions computed in the model $\sigma(\mathbf{x})$, and $C.C.$ denotes the complex conjugate of the first part of the expression. The \pm comes from the reciprocity

theorem for electromagnetic Green's functions used in eq. 4. A +(-) is used for F=H(E). This approach to gradient calculation is equivalent to the approach published by Tarantola (1984).

The first Green's function in eq. 4 is obtained by recording the electric field in the n direction at position \mathbf{x} , due to a unit source in the i direction at position \mathbf{x}_r , throughout the model space. For $F=E(H)$, $S=J(M)$, and denotes an electric(magnetic) source. The kernel in the sum over source positions is equivalent to a recording of the n component of the electric field at position \mathbf{x} due to a source at position \mathbf{x}_s , in the same direction as \mathbf{J} . The amplitude for this source is given by

$$S_{ik}(\omega) = W^F(\vec{x}_r|\vec{x}_s; \omega) \Delta F_i^*(\vec{x}_r|\vec{x}_s; \vec{J}, \omega) J_k(\vec{x}_s; \omega). \quad (5)$$

Since Maxwell's equations are linear with respect to the source term, the sum over source positions in eq. 4 can be computed in one modeling step by using multiple sources where the complex amplitude of each source is given by eq. 5.

Gradient calculation using a fast finite-difference time-domain method

We are currently using a fast finite-difference time-domain (FDTD) method for modeling the electromagnetic fields in the subsurface described by a 3D conductivity model. The method is described in detail by Maaø (2007). An important obstacle for efficiently solving equations for geophysical problems with a FDTD method is the wide range of velocities involved in the problem. To tackle this, we employ a mathematical transform of the original problem to reduce the frequency dependence of the transformed problem. This results in a formidable decrease in computational time. After the transformed problem has been solved, the data are transformed to the frequency domain using a Fourier transform with a complex frequency, yielding frequency domain data which satisfies the original problem.

This modeling approach represents a challenge when computing gradients of the misfit functional using eq. 4. The complex source amplitude needed in the backward-propagating step in the gradient computation is specified in the frequency domain. The transform between the original-problem frequency domain and the modified-problem time domain where we perform the FDTD computation is for the computed E fields given by

$$E(\omega) = \frac{\omega'}{\omega} \int dt' E(t') \exp[i\omega' t'] = \frac{f(\omega)}{\omega} \int dt' E(t') \exp[if(\omega)t'], \quad (6)$$

where

$$i\omega'(1 - i\omega'\alpha) = i\omega, \quad (7)$$

and α is a parameter in the transform. The transform of the sources between the modified-problem time domain and the original-problem frequency domain is

$$S(\omega) = \int dt' S(t') \exp[i\omega' t'] = \int dt' S(t') \exp[if(\omega)t']. \quad (8)$$

In order to find a representation of $S(t')$, which satisfies Eq. 8, we write the relation in matrix form,

$$S_\omega = A_{\omega'} S_{t'}. \quad (9)$$

Singular-value decomposition (SVD) is then used to find a well-behaved inverse to A enabling the calculation of $S_{t'}$ from the vector S_ω containing the complex amplitude of the source at all the frequencies of interest.

Test of gradient calculations on synthetic data

The gradient calculation is tested on synthetic data from 7 receivers using the reference model in fig. 1. The reference model consists of a 1- Ωm homogeneous formation starting at 750 meters water depth. A high-resistive box-formed anomaly is introduced at 1800 m depth below the sea surface. The anomaly has a resistivity of 25 Ωm , and dimensions 5km x 4km x 300m in the x-, y-, and z-direction respectively. The receivers are placed at the seafloor along a line in the x direction over the middle of the anomaly. Using the synthetic data from the reference model as observed data, we compute the gradient of the misfit functional for two different models.

Model I has the same geometry as the reference model, but contains a 10- Ωm anomaly. When Green's functions for this model are used in eq. 4, we expect a positive gradient within the volume of the anomaly since the anomaly's resistivity in model I is lower than for the reference model. Using eq. 4, the gradients are computed for each receiver. The gradients from all receivers are then stacked to yield the total gradient. Fig. 2(a) shows the gradient from the first receiver while fig. 2(b) shows the stacked gradients. As expected, the gradient has large positive values corresponding to the anomaly positioned correctly both in depth and along the axis following the receiver line.

Model II also has the same geometry as the reference model, but has a 50- Ωm anomaly. In this case the gradient is expected to have negative values within the volume of the anomaly. The stacked gradient is plotted in fig. 3 and we see the large negative values at the correct positions both in depth, and along the receiver line.

Finally, we show results from 3D inversion of the synthetic reference-model data using the data misfit and gradient from eqs. 1 and 4 as input to a quasi-Newton update algorithm (Byrd et al., 1995). The starting model for the inversion is a homogeneous 1 Ωm half-space model. The misfit functional in eq. 1 is computed from inline, electric fields using one frequency (0.25 Hz). Data from source-receiver offsets between 1 km and 4.5 km go into the misfit. Observation of equation 4 shows that due to the muting of short-offset data, the gradient at positions close to the receiver is dominated by the Green's function for a source in the receiver position and carries little information about the reference model. The gradient for a single receiver in fig. 2(a) clearly shows that it is dominated by the receiver-position Green's function close to the receiver. Figure 2(b) shows that when the gradients from all receivers are stacked, the near-receiver effect gives rise to a variation between positive values for the gradient in close proximity of the receivers and negative values for the gradient between the receivers. Since this kind of variation can cause problems in the inversion by introducing non-physical variations in the resistivity model close to the receivers, we choose to mute gradients around the receivers prior to stacking. We also choose not to update the topmost formation layer of the model, since variations in the model close to the seafloor can greatly influence the synthetic data.

Plots of the resistivity model and corresponding gradients for a few iterations in the inversion are shown in fig. 4. We see that after no more than 30 iterations, the model has converged to a high-resistive anomaly positioned correctly in the transversal direction compared to the reference-model anomaly. The center of the inverted anomaly is at about 1700 m in depth, which is 250 m shallower than the reference-model anomaly. The gradient at iteration 30 indicates that further updates will increase the resistivity in the area where the high-resistive anomaly has appeared in the inversion model. At iteration 80 the resistivity of the anomaly has indeed increased, but the position and shape of the inverted anomaly has not changed much. The resistivity of the reference-model anomaly was 25 Ωm . The maximum value obtained for the inverted anomaly is 11 Ωm .

The inversion model in the presented example has dimensions 18km x 10km x 3km and grid cells of size 150m x 150m x 150 m. The forward modelling was carried out on models of approximate size 10km x 10km x 3km. For the presented inversion results, iteration 30 was reached after four hours.

Conclusions

We have presented calculation of the gradient of the misfit functional for 3D inversion of marine CSEM data based on our fast FDTD algorithm, and showed that it is well-behaved for a synthetic-data example. One benefit of using a time-domain approach is that fields for several frequencies are obtained from one forward modelling thus saving valuable computational resources when inverting a large number of receivers.

Acknowledgements

We acknowledge valuable discussions and contributions from our colleagues Astrid K. Bjørke and Rune Mittet.

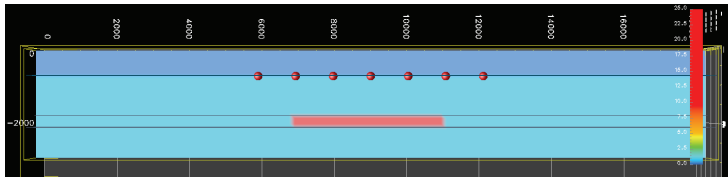


Fig. 1: The reference model used to generate the “observed data” used in the gradient computation. The red spheres indicate the receiver positions. The horizontal lines mark depths 750m (seafloor), 1800m (top edge of anomaly), and 2100m (deep edge of anomaly).

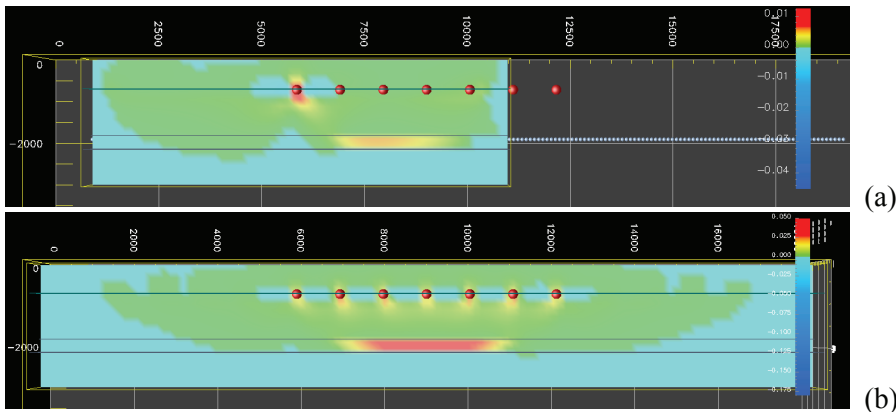


Fig. 2: The misfit gradient for a model having a 10-Ωm anomaly co-located with the anomaly in the reference model.(a):Gradient from the first receiver. (b): Stacked gradients from all receivers. Red: large, positive values, Green: small positive values, Light-blue: small negative values, Dark-blue: large negative values.

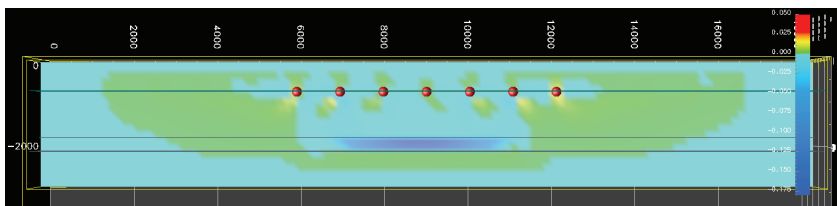
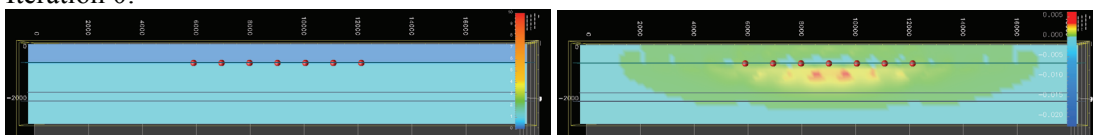
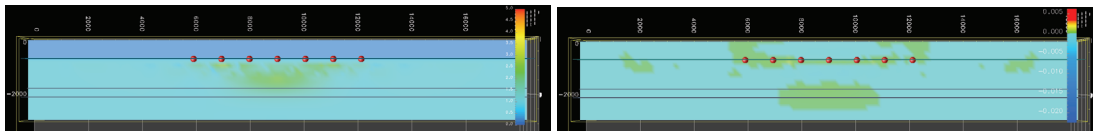


Fig. 3: As Fig. 2, but with a 50-Ωm anomaly.

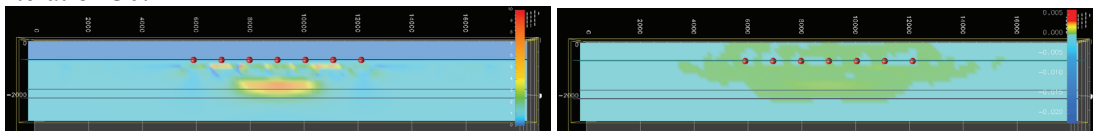
Iteration 0:



Iteration 10:



Iteration 30:



Iteration 80:

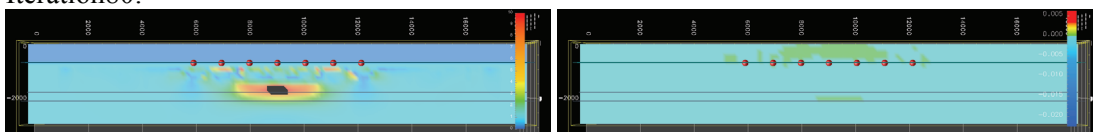


Fig. 4: The model(left) and resulting misfit gradient(right) for some iterations in the inversion.

References

- Byrd, R.H., Lu, P. and Nocedal, J. [1995] A Limited Memory Algorithm for Bound Constrained Optimization. *SIAM Journal on Scientific and Statistical Computing*, **16**(5), 1190-1208.
- Eidesmo, T., Ellingsrud, S., MacGregor, L. M., Constable, S., Sinha, M. C., Johansen, S. Kong, F. N. and Westerdahl, H. [2002] Sea bed logging (SBL) a new method for remote and direct identification of hydro carbon filled layers in deepwater areas. *First Break*, **20**, 144-152.
- Gribenko, A. and Zhdanov, M. [2007] Rigorous 3D inversion of marine CSEM data based on the integral equation method. *Geophysics*, **72**(2), WA73-WA84.
- Maaø, F. A. [2007] Fast finite-difference time-domain modeling of marine-subsurface electromagnetic problems. *Geophysics*, **72**(2), A19-A23.
- Mittet, R., Løseth, L., Ellingsrud, S. [2004] Inversion of SBL data acquired in shallow waters. *66th EAGE Conference & Exhibition*, Extended Abstracts, E020.
- Newmann, G. A. and Alumbaugh, D. L. [1997] Electromagnetic modeling and inversion on massively parallel computers. In: Oristaglio, M. and Spies, B. (Eds.) *Three dimensional electromagnetics*, SEG.
- Plessix, R.-E. and Van der Sman, P. [2007] 3D CSEM modeling and inversion in complex geological settings. *SEG Annual Meeting*, Extended Abstracts, 589-593.
- Roth, F. and Zach, J. J. [2007] Inversion of marine CSEM data using up-down wavefield separation and simulated annealing. *SEG Annual Meeting*, Extended Abstracts, 524-528.
- Spies, F. N., MacDonald, K. C., Atwater, T., Ballard, R., Caranza, A., Cordoba, D., Cox, C. Garcia, V. M. D., Francheteau, J., Guerrero, J., Hawkings, J., Haymon, R., Hessler, R., Juteu, T., Kastner, M., Larson, R., Luyendyk, B., MacDougall, J. D., Miller, S., Normark, W., Orcutt, J. and Rangin, C. [1980] East Pacific Rise: Hot springs and geophysical experiments. *Science*, **207**, 1421-1433.
- Tarantola, A. [1984] Inversion of seismic reflection data in the acoustic approximation. *Geophysics*, **49**(8), 1259-1266.